NASA/TM—2019–220048

TESS Data Release Notes:
Sector 5, DR7

Michael M. Fausnaugh, Christopher J. Burke
Kavli Institute for Astrophysics and Space Science, Massachusetts Institute of Technology,
Cambridge, Massachusetts

Douglas A. Caldwell
SETI Institute, Mountain View, California

Jon M. Jenkins
Ames Research Center, Moffett Field, California

Jeffrey C. Smith, Joseph D. Twicken
SETI Institute, Mountain View, California

Roland Vanderspek
Kavli Institute for Astrophysics and Space Science, Massachusetts Institute of Technology,
Cambridge, Massachusetts

John P. Doty
Noqsi Aerospace Ltd, Billerica, Massachusetts

Eric B. Ting
Ames Research Center, Moffett Field, California

Joel S. Villasenor
Kavli Institute for Astrophysics and Space Science, Massachusetts Institute of Technology,
Cambridge, Massachusetts

February 27, 2019

Acknowledgements

This report is available in electronic form at
https://archive.stsci.edu/tess/

---

[1] https://archive.stsci.edu/missions/tess/doc/EXP-TESS-ARC-ICD-TM-0014.pdf
[2] https://archive.stsci.edu/kepler/manuals/KSCI-19081-002-KDPH.pdf

1 Observations

TESS Sector 5 observations include physical orbits 17 and 18 of the spacecraft around the Earth. Data collection was paused for 1.35 days during perigee passage while downloading data. The use of Camera 1 in attitude control was disabled for the last ~ 0.5 days of orbit 18 due to strong scattered light signals (see §1.2), and data taken with Camera 1 during this period were excluded from the pipeline analysis (see §2). In total, there are 25.23 days of science data collected in Sector 5.

Table 1: Sector 5 Observation times

	UTC	TJD[a]	Cadence #
Orbit 17 start	2018-11-15 07:47:48	1437.82566	151467
Orbit 17 end	2018-11-27 16:44:46	1450.19856	160375
Orbit 18 start	2018-11-29 01:09:22	1451.54898	161347
Camera 1 Guiding Disabled	2018-12-11 10:31:39	1463.93945	170269
Orbit 18 end	2018-12-11 21:35:39	1464.40056	170601

[a] TJD = TESS JD = JD - 2,457,000.0

The spacecraft was pointing at RA (J2000): 73.5382°; Dec (J2000): $-31.9349°$; Roll: 191.05°. Two-minute cadence data were collected for 20,000 targets, and full frame images were collected every 30 minutes. See the TESS project Sector 5 observation page[3] for the coordinates of the spacecraft pointing and center field-of-view of each camera, as well as the detailed target list. Fields-of-view for each camera with all two-minute targets can be found at the TESS Guest Investigator Office observations status page[4].

1.1 Notes on Individual Targets

Four very bright stars (Tmag $\lesssim 2$) with large pixel stamps were not processed in the photometric pipeline. Target pixel files with raw data are provided, but no light curves were produced. The affected TIC IDs are 255559489, 231308237, 38877693, and 325685265.

Two targets, 300015238 and 300015239, lie within one pixel of each other. The contaminating flux for these objects is very large, and the pipeline assigns them disjoint photometric apertures, which likely causes uncorrected systematic errors in the light curves.

One target (220393543) had a small aperture selected (25x25 pixels) that did not fully capture the bleed trails.

1.2 Spacecraft Pointing and Momentum dumps

The reaction wheel speeds were reset with momentum dumps every 3.0 days. FFIs taken during these times are marked with bit 6 (Reaction Wheel Desaturation Events) set. Only one or two FFIs are affected by each momentum dump.

---

[3] https://tess.mit.edu/observations/sector-5
[4] https://heasarc.gsfc.nasa.gov/docs/tess/status.html

At the end of orbit 18, the Earth was $< 35°$ from the boresight of Camera 1. At these low angles, the level of scattered light is too high for meaningful guide star centroids to be measured. Guiding with Camera 1 was therefore disabled at this time, starting at TJD 1463.93945 until the end of the sector. When Camera 1 guiding was disabled, the spacecraft attitude shifted by a small amount, about 1 arc-second (0.05 pixels).

Figure 1 summarizes the pointing performance over the course of the sector based on Fine Pointing telemetry. Disabling Camera 1 guiding near the end of the Sector caused a brief impulse in pointing, which settled out within minutes. The other periods of increased dispersion are generally correlated with the momentum dumps. Several shorter impulse-like events are also evident, which are associated with quasi-instantaneous changes in the internal friction of the reaction wheels.
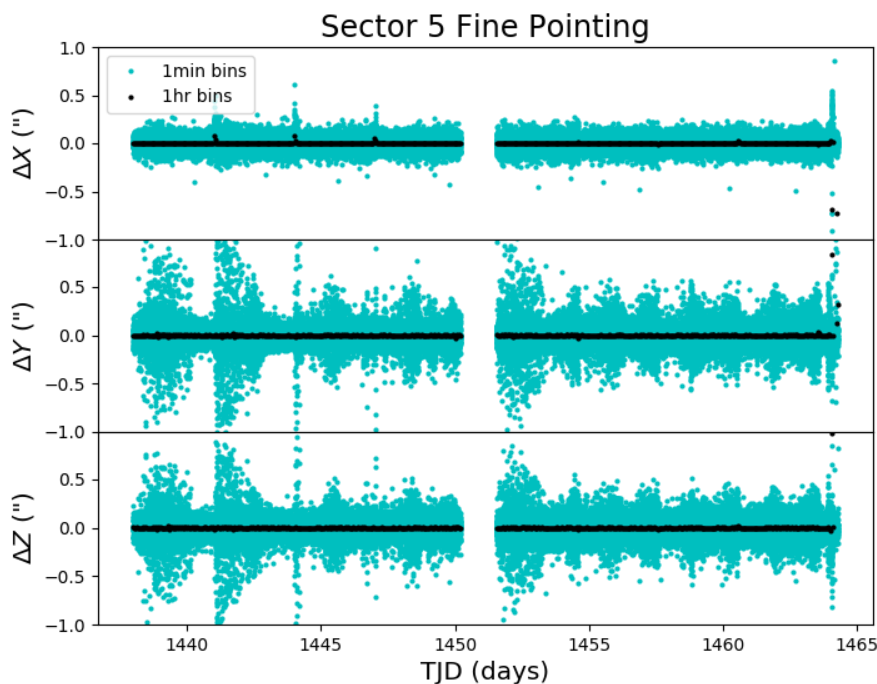

Figure 1: Guiding corrections based on spacecraft fine pointing telemetry. The delta-quaternions from each camera have been converted to spacecraft frame, binned to 1 minute and 1 hour, and averaged across cameras. Long-term trends (such as those caused by differential velocity aberration) have also been removed. The $\Delta X/\Delta Y$ directions represent offsets along the the detectors' rows/columns, while the ΔZ direction represents spacecraft roll. The brief period of large dispersion at the end of the sector is caused by disabling Camera 1 for guiding (see §1).

1.3   Scattered Light

Figure 2 shows the median value of the background estimate for all targets on a given CCD as a function of time. Figure 3 shows the angle between each camera's boresight and the Earth or Moon—this figure can be used to identify periods affected by scattered light and

the relative contributions of the Earth and Moon to the image backgrounds. In Sector 5,the main stray light features are caused by the Earth rising above the sunshade at the end of each orbit, and strong glints appear during these times. As noted in §1.2, the Earth moves quite close to the boresight of Camera 1 at the end of orbit 18.
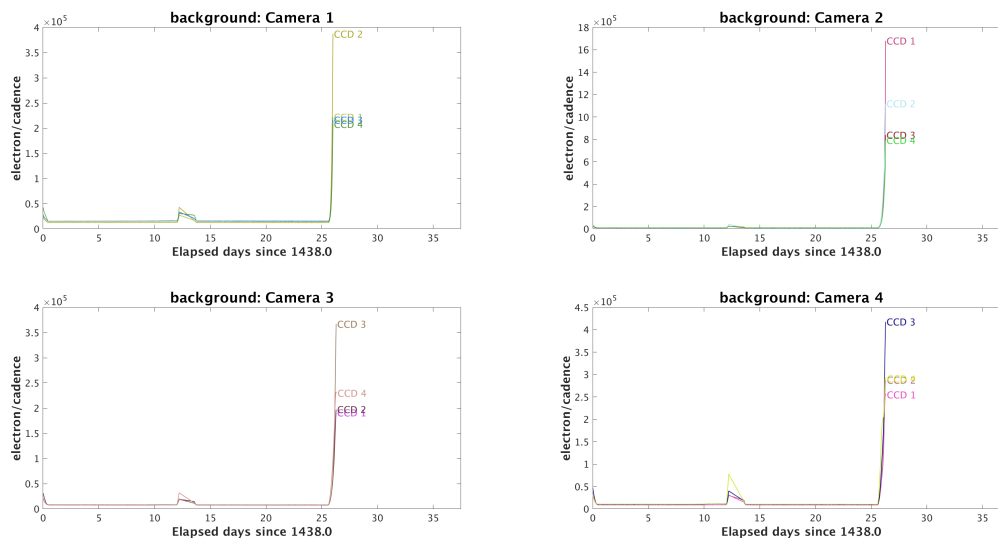

Figure 2: Median background flux across all targets on a given CCD in each camera. The changes are caused by variations in the orientation and distance of the Earth and Moon. The upturn at the end of each orbit is caused by the Earth rising above the sunshade.

2 Data Anomaly Flags

See the SDPDD (§9) for a list of data quality flags and the associated binary values used for TESS data, and the Instrument Handbook for a more detailed description of each flag.

The following flags were not used in Sector 5: bits 2, 7, 9, and 11 (Safe Mode, Cosmic Ray in Aperture, Discontinuity, and Cosmic Ray in Collateral Pixel).

Cadences marked with bits 1, 3, 4, 6, and 12 (Attitude Tweak, Coarse Point, Earth Point, Reaction Wheel Desaturation Event, and Straylight) were marked based on spacecraft telemetry.

Cadences marked with bit 5 and 10 (Argabrightening Events and Impulsive Outlier) were identified by SPOC pipeline results. Bit 5 marks a sudden change in the background measurements. In practice, bit 5 flags are caused by rapidly changing glints and unstable pointing at times near momentum dumps. Bit 10 marks an outlier identified by PDC and omitted from the cotrending procedure.

Cadences marked with bit 8 (Manual Exclude) are ignored by PDC, TPS, and DV for cotrending and transit searches. In Sector 5, these cadences were identified using spacecraft telemetry from the fine pointing system. All cadences with pointing excursions >21 arcseconds (∼1 pixel) were flagged for manual exclude. See Figure 4 for an assessment of the performance of the detrending based on the final set of manual excludes.
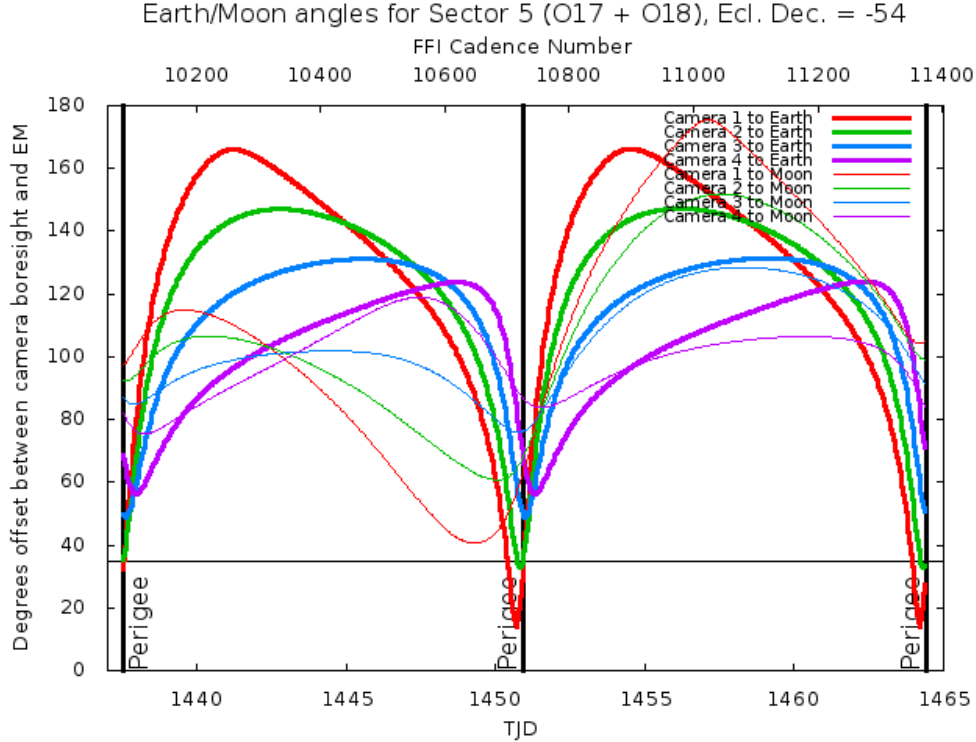
4

Figure 3: Angle between the four camera boresights and the Earth/Moon as a function of time. When the Earth/Moon moves within ~35° of a camera's boresight, scattered light patterns and complicated features such as glints may appear. At larger angles, low level patchy features may appear. This figure can be used to identify periods affected by scattered light and the relative contributions of the Earth and Moon to the background. However, the background intensity and locations of scattered light features depend on additional factors, such as the Earth/Moon azimuth and distance from the spacecraft.

FFIs were only marked with bit 6 and 12 (Reaction Wheel Desaturation Events and Straylight). Only one or two FFIs are affected by each momentum dump.

Due to the scattered light in Camera 1 at the end of orbit 18, the data from cadences 170313 to 170601 (the end of the sector) from Camera 1 were manually excluded from the pipeline analysis. These cadences for targets in Camera 1 are marked with bit 12 (Straylight) and set to NULL in the light curve files. Raw and flux-calibrated pixels for these cadences are provided in the target pixel files, but no photometry or centroid positions were calculated.

3 Anomalous Effects

3.1 Smear Correction Issues

1. Camera 4, CCD 4, Columns 431–437: There is a bright star in the upper buffer rows, which bleeds slightly into the upper serial register and effects the smear rows in this column.

We have identified some moderately bright stars in the upper buffer rows that affect the first
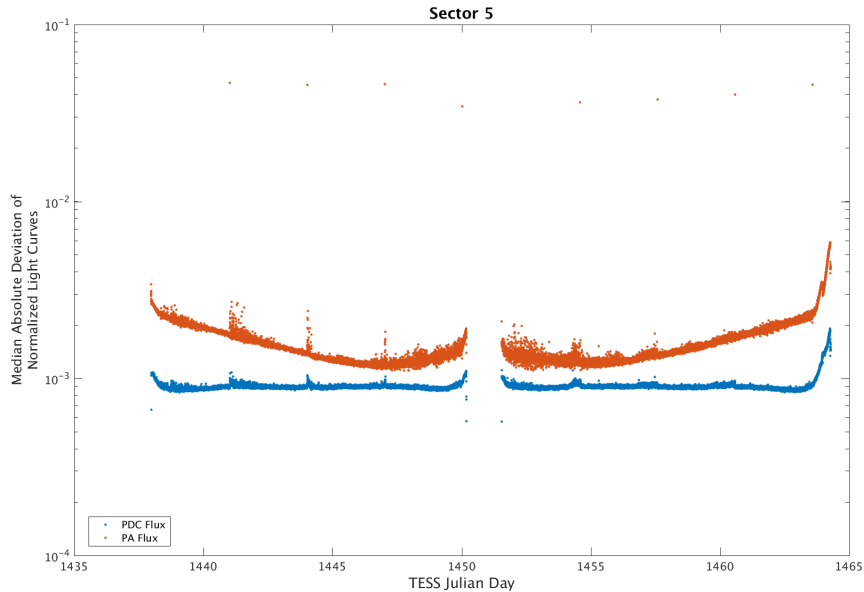
Figure 4: Median absolute deviation (MAD) for the 2-minute cadence data from Sector 5, showing the performance of the cotrending after identifying Manual Exclude data quality flags. The MAD is calculated in each cadence across stars with flux variations less than 1% for both the PA (red) and PDC (blue) light curves, where each light curve is normalized by its median flux value. The scatter in the PA light curves is much higher than that for the PDC light curves, and the outliers in the PA light curves are largely absent from the PDC light curves due to the use of the anomaly flags. Note that the first and last cadences in each orbit are treated as gaps by PDC.

row of the virtual smear region. However, the smear correction is robust against these cases.

3.2 Black Flutter

Flutter in the mean black level was observed in two cameras during Sector 5: camera 2, CCD 2, all outputs, cadences 152300–153000 and 162000–163000; and camera 4, CCD 2, output D, cadences 155450–156660.

Popcorn noise in the mean black level was observed in three cameras during Sector 5: camera 1, CCD 3, output C, cadences 155190–157700; camera 3, CCD 1, output B, throughout the sector; and camera 4, CCD 1, output A, throughout the sector. See the Instrument Handbook §6.3.4 & 6.3.5 for more details about overclock popcorn noise and flutter.

3.3 Fireflies and Fireworks

Table 2 lists all firefly and fireworks events for Sector 5. These phenomena are small, spatially extended, comet-like features in the images that may appear one or two at a time (fireflies) or in large groups (fireworks). See the Instrument Handbook for a complete description.
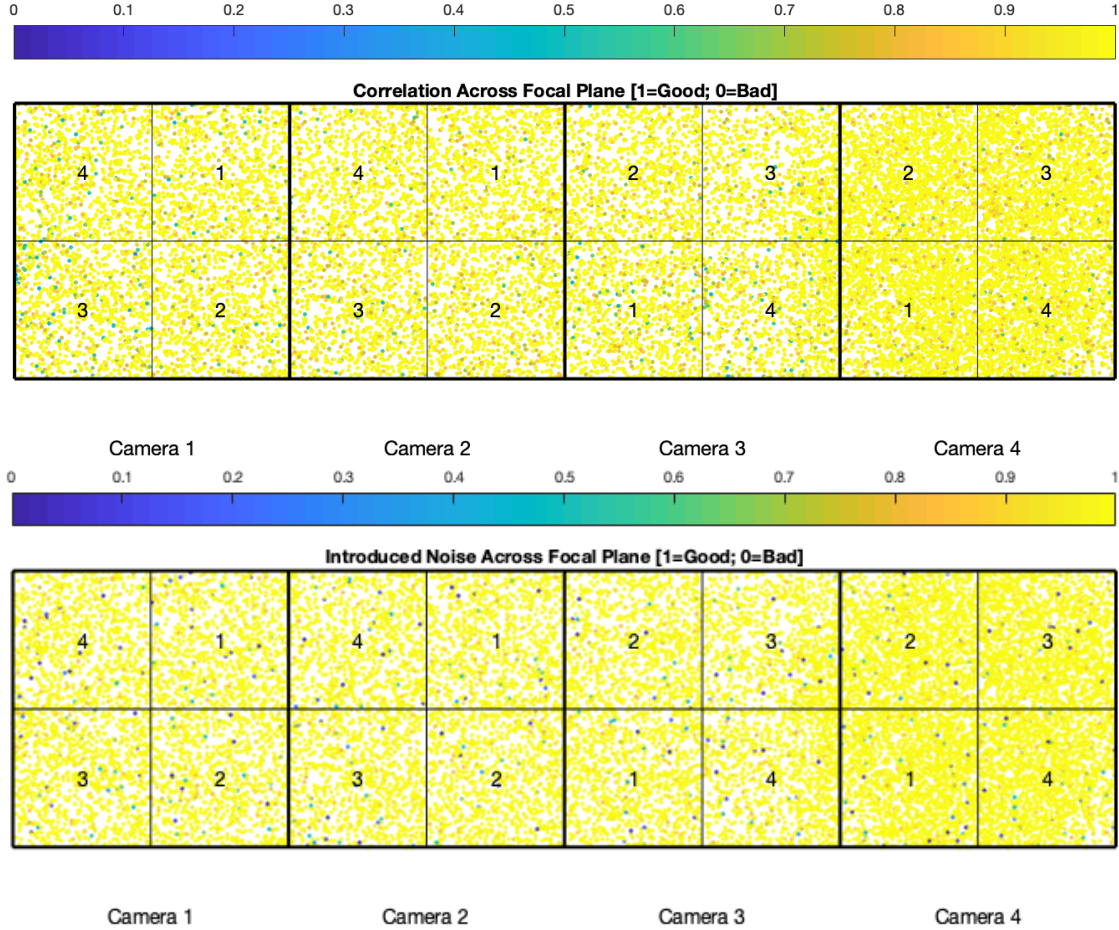
6

Figure 5: PDC residual correlation goodness metric (top panel) and PDC introduced noise goodness metric (bottom panel). The metric values are shown on a focal plane map indicating the camera and CCD location of each target. The correlation goodness metric is calibrated such that a value of 0.8 means there is less than 10% mean absolute correlation between the target under study and all other targets on the CCD. The introduced noise metric is calibrated such that a value of 0.8 means the power in broad-band introduced noise is only slightly above the level of uncertainties in the flux values.

3.4   TJD Calculation

The spacecraft clock drifts slowly relative to UTC time at a rate of ∼35 milliseconds per day. This drift is captured in a clock kernel that is used to calculate TJD from spacecraft time. The calculated clock kernel correcting this difference is based on the measured drift rate from periodic S-band and Ka-band ranging contacts.

The clock kernel used to calculate TJD in Sector 5 used ranging data collected only through late August, 2018; as a result, the extrapolation to Sector 5 times is slightly off. The error between true and calculated times grew linearly with time since August 2018, so that the calculated TJD values in all data products are offset from the correct values by ∼1.7 seconds at the end of orbit 18 (2018-12-11 UTC). This error also implies that the durations of the individual cadences are underestimated by about 20 microseconds and the FFIs are
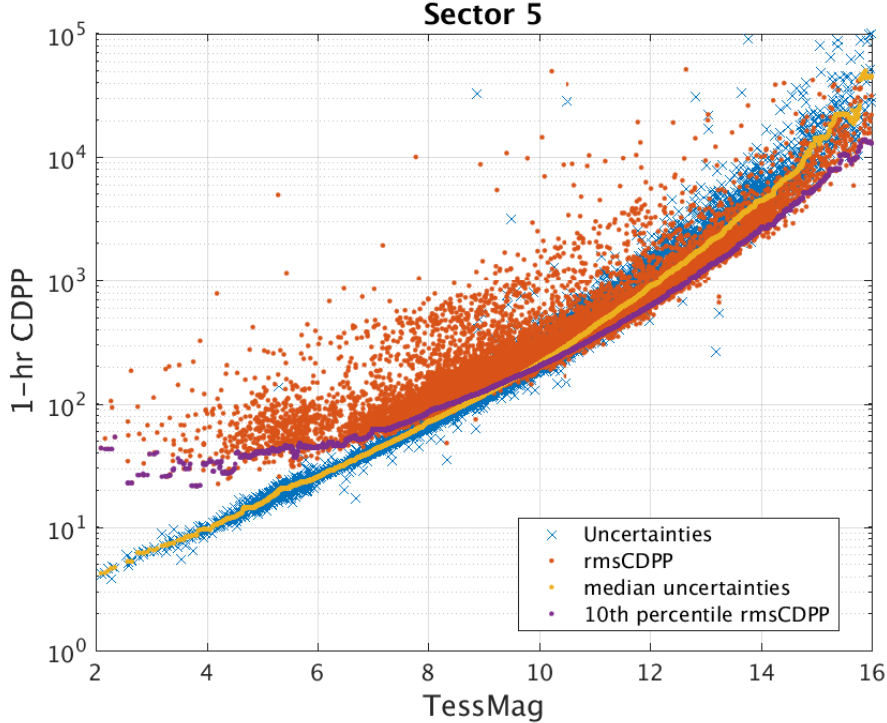
Figure 6: 1-hour CDPP. The red points are the RMS CDPP measurements for the 19,996 light curves from Sector 5 plotted as a function of TESS magnitude. The blue x's are the uncertainties, scaled to 1-hour timescale. The purple curve is a moving 10th percentile of the RMS CDPP measurements, and the gold curve is a moving median of the 1-hr uncertainties.

low by about 280 microseconds, as calculated by the difference between the TSTOP and TSTART times. This issue will be corrected if the data are reprocessed in a future data release.

4 Pipeline Performance and Results

4.1 Change in 1-D Black Correction

Starting with Sector 5 processing, the SPOC pipeline 1-D Black correction has been changed to a two-component model from the polynomial fit that had been used prior (see the Sector-1 Data Release Notes, § 3.9[5], for a discussion of issues with the polynomial fit). The new black model consists of two components: a time-varying correction and a static row-by-row correction. The time-varying component is the robust mean of the selected overclock columns and rows for each cadence. After removing the time-varying mean black level, the row correction contains one value for each row and is the robust mean over columns and time. The 1-D black correction ignores the first column of each overclock region, which can be contaminated by flux from the imaging pixels. The time-varying component of the model

---

[5]https://archive.stsci.edu/missions/tess/doc/tess_drn/tess_sector_01_drn01_v01.pdf

Table 2: Sector Fireflies and Fireworks

FFI Start	FFI End	Cameras	Description
2018319172939	2018319182939	1, 2, 3	Fireflies
2018321095939	2018321102939	2, 3, 4	Fireflies
2018324152939	2018324155939	2, 4	Fireflies
2018325082939	2018325085939	3, 4	Firefly
2018327185939	2018327192939	1, 2, 3	Fireflies
2018328092939	2018328095939	1, 2, 3	Firefly
2018333052939	2018333055939	1	Firefly
2018335185939	2018335192939	1, 2, 3, 4	Fireworks
2018336125939	2018336132939	3	Firefly
2018338085939	2018338092939	2	Firefly
2018338185939	2018338192939	3	Firefly
2018339002939	2018339005939	4	Firefly

removes cadence-to-cadence black variations as well as the black flutter and popcorn noise seen on some CCDs. The static row-dependent component is designed to correct the "tired chain" effect (TESS Instrument Handbook §6.8.5) where bright illuminated pixels cause an increase in the black level of subsequent pixels. The updated model removes this small (~ 10 ADU/cadence) residual bias.

4.2   Light Curves and Photometric Precision

Figure 5 gives the PDC goodness metrics for residual correlation and introduced noise on a scale between 0 (bad) and 1 (good). The performance of PDC is very good and generally uniform over most of the field of view. This is the first data release in which the goodness metrics reported in the light curve files match the calibrated values shown in Figure 5.

Figure 6 shows the achieved Combined Differential Photometric Precision (CDPP) at 1-hour timescales for all targets. The measured CDPP values level out between 20 and 30 ppm at the bright end, and the residual error after accounting for known sources of uncertainty (photon noise in the target and background, read noise, etc.) is about the same down to Tmag = 10–11. The uncertainties at lower magnitudes are probably somewhat overestimated, perhaps due to crowding/blends and other sources of excess light in the photometric aperture.

4.3   Transit Search and Data Validation

In Sector 5, the light curves of 19,996 targets were subjected to the transit search in TPS. Of these, Threshold Crossing Events (TCEs) at the 7.1σ level were generated for 829 targets. Cadences at the end of orbit 18, from 170013 to 170519, were excluded from the transiting planet search due to the effects of rapidly changing scattered light and glints (see Figure 2). Cadences near the first and second-to-last momentum dump also caused an inordinate number of TCEs on an initial run of TPS. Approximately 16 hours around those times were also

excluded from the planet search, in order to reduce the number of false positives. These periods extended from cadence 153522 to 154022 and 167607 to 168107.

The top panel of Figure 7 shows the distribution of orbital periods for the TCEs found in Sector 5. There is an excess of TCEs at periods near 10.5 and 14 days. These periods are mainly caused by the spacing of momentum dumps between the first and second orbit, as shown by Figure 8—the isolated peak in the first orbit near the second momentum dump is separated from the peaks in the second orbit by ∼10.5 and 14 days. The slight depressions in Figure 8 near the first momentum dump, the second-to-last momentum dump, and the very end of the sector mark the periods excluded for the planet search, described above.

The vertical histogram in the right panel of Figure 7 shows the distribution of transit depths derived from limb-darkened transiting planet model fits for TCEs. The model transit depths range down to the order of 100 ppm, but the bulk of the transit depths are considerably larger.

A search for additional TCEs in potential multiple planet systems was conducted in DV through calls to TPS. A total of 1248 TCEs were ultimately identified in the SPOC pipeline on 829 unique target stars. Table 3 provides a breakdown of the number of TCEs by target. Note that targets with large numbers of TCEs are likely to include false positives.

Table 3: Sector 5 TCE Numbers

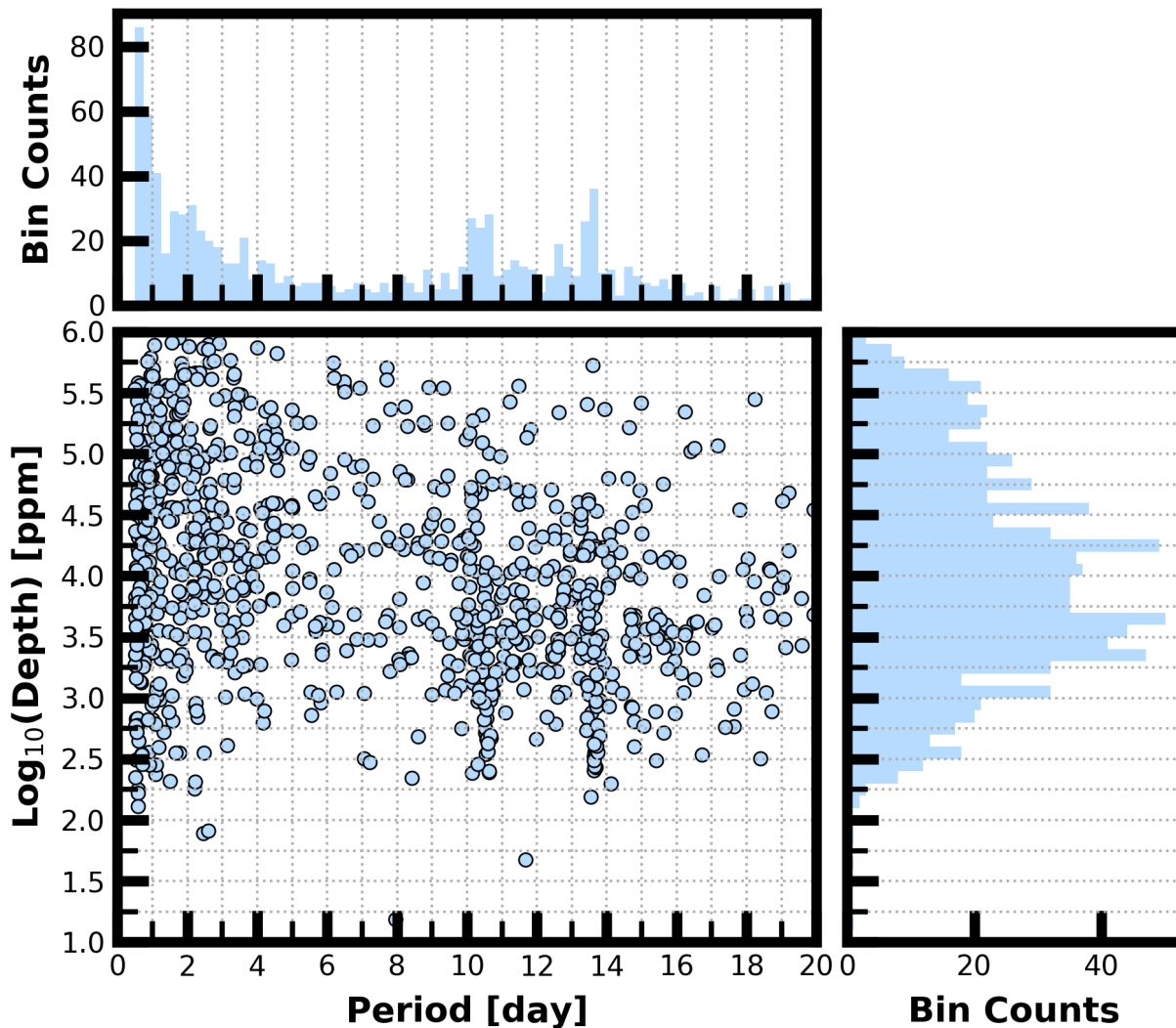| Number of TCEs	Number of Targets	Total TCEs
1	505	505
2	246	492
3	66	198
4	9	36
5	1	5
6	2	12
–	829	1248

Figure 7: Lower Left Panel: Transit depth as a function of orbital period for the 1248 TCEs identified for the Sector 5 search. For enhanced visibility of long period detections, TCEs with orbital period <0.5 days are not shown. Reported depth comes from the DV limb darkened transit fit depth when available, and when not available, the DV trapezoid model fit depth. Top Panel: Orbital period distribution of the TCEs shown in the lower left panel. Right Panel: Transit depth distribution for the TCEs shown in the lower left panel.
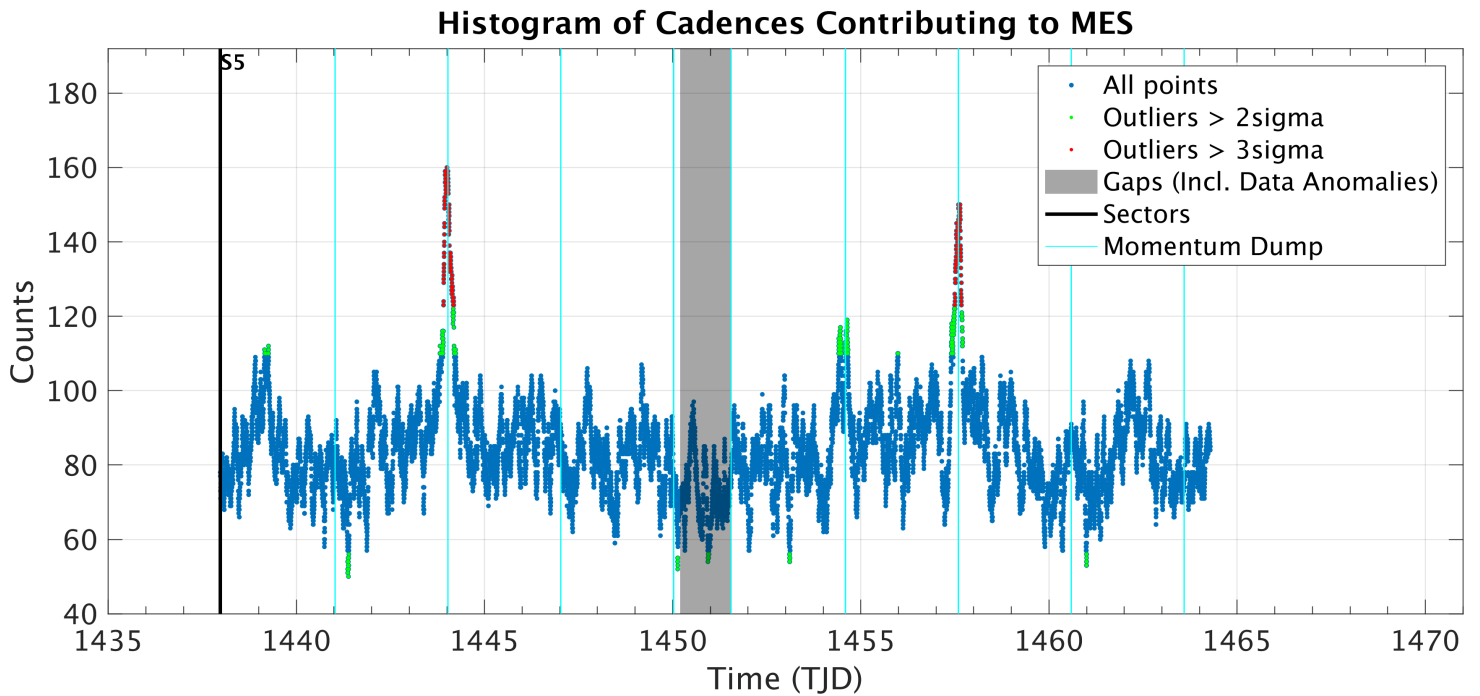
Figure 8: Number of TCEs at a given cadence exhibiting a transit signal. Isolated peaks are caused by a single event and result in spurious TCEs. The peaks typically align with pointing instabilities and strong background variations. The main features to be aware of are cadences impacted by momentum dumps (e.g., TJD epochs 1444.0 & 1457.5).

References

Jenkins, J. M. 2017, Kepler Data Processing Handbook: Overview of the Science Operations Center, Tech. rep., NASA Ames Research Center

Jenkins, J. M., Twicken, J. D., McCauliff, S., et al. 2016, in Proc. SPIE, Vol. 9913, Software and Cyberinfrastructure for Astronomy IV, 99133E

Li, J., Tenenbaum, P., Twicken, J. D., et al. 2019, *PASP*, 131, 024506

Twicken, J. D., Catanzarite, J. H., Clarke, B. D., et al. 2018, *PASP*, 130, 064502

Vanderspek, R., Doty, J., Fausnaugh, M., et al. 2018, TESS Instrument Handbook, Tech. rep., Kavli Institute for Astrophysics and Space Science, Massachusetts Institute of Technology

Acronyms and Abbreviation List

BTJD Barycentric-corrected TESS Julian Date

CAL Calibration Pipeline Module

CBV Cotrending Basis Vector

CCD Charge Coupled Device

CDPP Combined Differential Photometric Precision

COA Compute Optimal Aperture Pipeline Module

CSCI Computer Software Configuration Item

CTE Charge Transfer Efficiency

Dec Declination

DR Data Release

DV Data Validation Pipeline Module

DVA Differential Velocity Aberration

FFI Full Frame Image

FIN FFI Index Number

FITS Flexible Image Transport System

FOV Field of View

FPG Focal Plane Geometry model

KDPH Kepler Data Processing Handbook

KIH Kepler Instrument Handbook

KOI Kepler Object of Interest

MAD Median Absolute Deviation

MAP Maximum A Posteriori

MAST Mikulski Archive for Space Telescopes

MES Multiple Event Statistic

NAS NASA Advanced Supercomputing Division

PA Photometric Analysis Pipeline Module

PDC Pre-Search Data Conditioning Pipeline Module

PDC-MAP Pre-Search Data Conditioning Maximum A Posteriori algorithm

PDC-msMAP Pre-Search Data Conditioning Multiscale Maximum A Posteriori algorithm

PDF Portable Document Format

POC Payload Operations Center

POU Propagation of Uncertainties

ppm Parts-per-million

PRF Pixel Response Function

RA Right Ascension

RMS Root Mean Square

SAP Simple Aperture Photometry

SDPDD Science Data Product Description Document

SNR Signal-to-Noise Ratio

SPOC Science Processing Operations Center

SVD Singular Value Decomposition

TCE Threshold Crossing Event

TESS Transiting Exoplanet Survey Satellite

TIC TESS Input Catalog

TIH TESS Instrument Handbook

TJD TESS Julian Date

TOI TESS Object of Interest

TPS Transiting Planet Search Pipeline Module

UTC Coordinated Universal Time

XML Extensible Markup Language